Kohn Anomalies in Tungsten and Other Cr-Group Metals

T. M. RICE AND B. I. HALPERIN*
Bell Telephone Laboratories, Murray Hill, New Jersey 07974
(Received 2 September 1969)

A detailed examination is made of the series of Kohn anomalies near the H point of the Brillouin zone of tungsten, arising from the "nesting" of the electron jack and hole octahedron. An analytic model of the Fermi surface, introduced by Girvan, Gold, and Phillips to fit their de Haas–van Alphen data, is employed. The electron susceptibility is evaluated and its maximum is found to occur at a sharp peak. The effect of the Kohn anomalies on the phonon spectrum and lifetime is estimated. Applications to other Cr-group metals are briefly considered.

I. INTRODUCTION

THE combination of accurate experimental information from the de Haas–van Alphen effect and good band-structure calculations has led to a detailed knowledge of the band structures of many metals. In recent years there has been considerable interest in using this information to determine band-structure effects on the wave-vector-dependent generalized susceptibility of metals.[1] It is generally accepted that such band-structure effects are responsible for the itinerant antiferromagnetism in Cr and for the incommensurate periods of the antiferromagnetism in many rare earth metals. Kohn[2] has shown that for a free-electron gas, the existence of a sharp Fermi surface leads to nonanalyticities in wave-vector-dependent quantities such as the phonon spectrum, susceptibilities, etc. These nonanalyticities are known as "Kohn anomalies." Subsequently, Taylor[3] and Roth, Zeiger, and Kaplan[4] considered the generalization of Kohn anomalies to arbitrary band structures. In particular, Roth *et al.*[4] showed that it is possible under certain conditions to have a "cusp"-type Kohn anomaly as distinct from the infinite slope or $x\log x$ singularity which occurs for a free-electron gas.

In this paper we examine in detail the nature of the Kohn anomalies near the H point of the Brillouin zone in tungsten. This is an especially interesting case for several reasons. It is known that there is a very large peak in the wave-vector-dependent susceptibility near the H point in the Cr-group metals arising from the "nesting" of the electron jack and the hole octahedron.[5] In Cr itself, of course, the total susceptibility diverges, leading to the antiferromagnetic phase transition. The one-electron susceptibility, however, remains finite. From a study of McWhan's results[6,7] on the vanishing of antiferromagnetism under pressure for a series of Cr-V and Cr-Mo alloys the present authors[6,7] suggested that the maximum in the one-electron susceptibility occurs at a "cusp"-type Kohn anomaly. The nature of the Kohn anomalies is determined by the shape of the Fermi surface, and in our study we use the analytic model of Girvan, Gold, and Phillips[8] for the tungsten Fermi surface. These authors have made a detailed study of the tungsten surface using the de Haas–van Alphen effect and have fit their data to an analytic model.

In Sec. II we study the positions and types of the Kohn anomalies in W along the ΓH line near the H point. These are obtained by computing the loci of intersection of two Fermi surfaces displaced relative to each other by a wave vector $\mathbf{Q}$, as a function of $\mathbf{Q}$. The anomalies occur at wave-vectors $\mathbf{Q}$ at which there are changes in connectivity in the loci of intersection. A series of three separate cusp-type anomalies and three ordinary anomalies are found near the H point.

In Sec. III a detailed calculation of the wave-vector-dependent one-electron susceptibility $\chi^0(\mathbf{Q})$ is described. Care is taken to treat accurately the contributions from regions near the Fermi surface which give rise to the nonanalyticities. We do not attempt to include accurately the contributions from other parts of the Brillouin zone. We ignore completely contributions from other bands, and we neglect all variations in the matrix elements. These effects may change the over-all magnitude of $\chi^0(\mathbf{Q})$, and will contribute a slowly varying background, but should not affect the fine structure arising from the shape of the Fermi surface.

The maximum of χ^0 is found to occur as a sharp peak at a $\mathbf{Q}$ value where the analysis in Sec. II shows a closely spaced group of one ordinary and two cusp-type anomalies. The combined anomaly behaves approximately like a single cusp-type anomaly. We have evaluated also the temperature dependence of the maximum value of χ^0 and we find it is in qualitative

---

* Address during the academic year 1969–1970: Department of Physics, Harvard University, Cambridge, Mass. 02138.

[1] W. E. Evenson and S. H. Liu, Phys. Rev. Letters **21**, 432 (1968); W. E. Evenson and S. H. Liu, Phys. Rev. **178**, 783 (1969); W. E. Evenson, G. S. Fleming, and S. H. Liu, *ibid.* **178**, 930 (1969).

[2] W. Kohn, Phys. Rev. Letters **2**, 393 (1959).

[3] P. L. Taylor, Phys. Rev. **131**, 1995 (1963).

[4] L. M. Roth, H. J. Zeiger, and T. A. Kaplan, Phys. Rev. **149**, 519 (1966).

[5] W. M. Lomer, Proc. Phys. Soc. (London) **80**, 489 (1962).

[6] T. M. Rice, B. I. Halperin, and D. B. McWhan, in Proceedings of the Eleventh International Conference on Low-Temperature Physics, p. 1308, 1969 (unpublished).

[7] T. M. Rice, A. S. Barker, B. I. Halperin, and D. B. McWhan, J. Appl. Phys. **40**, 1337 (1969).

[8] R. F. Girvan, A. V. Gold, and R. A. Phillips, J. Phys. Chem. Solids **29**, 1485 (1968).

agreement with that deduced from the study of the Néel temperature in Cr and its alloys.[6,7]

In Sec. IV we examine the phonon spectrum near the H point. We use an empirical formula to relate the phonon frequency to χ^0 and interpolate between the experimental points determined by Chen and Brockhouse.[9,10] The last authors measured the phonon frequencies on a mesh which is too coarse to resolve the fine structure which we predict. The principal feature of our results is a narrow dip in the phonon frequency centered at the point $(0.924,0,0)\times 2\pi/a$. Corresponding to the dip in the real part we find a peak in the imaginary part or inverse lifetime of the phonons

Finally, in Sec. V we briefly discuss the application of these results to the other Cr-group metals. In particular we show that at least one cusp-type anomaly must occur near the H point in the Cr-group metals.

II. POSITIONS AND TYPES OF KOHN ANOMALIES IN W

The Fermi surface of the Cr-group metals consists of several sheets. Lomer[5] pointed out that the wave-vector-dependent susceptibility will be greatly enhanced near the H point of zone by the "nesting" or "matching" property of the electron and hole pockets centered at Γ and H, respectively. The hole pocket at H is approximately octahedral in shape and is referred to as the hole octahedron. The electron pocket, called the "jack," has a "body" which is roughly octahedral and slightly smaller than the hole octahedron and has, in addition, six balls at the corners. The relative shapes of the two octahedral portions of the Fermi surface determine the structure of the Kohn anomalies. Girvan, Gold, and Phillips[8] have parametrized the shape of these surfaces for W. The hole octahedron is determined by the condition

$$W_0(\mathbf{k}+\tfrac{1}{2}\mathbf{G}_{100})=0, \tag{1}$$

where

$$W_0(\mathbf{k})=\frac{P_4{}^m}{|k_x|^m+|k_y|^m+|k_z|^m}-1 \tag{2}$$

and

$$m=P_5\sum_{i=x,\,y,\,z}\left[1-\left(\frac{k_i}{k}\right)^2\right]^{P_6}. \tag{3}$$

TABLE I. Parameters for the W Fermi surface from Ref. 7.

$P_4=0.38256(2\pi/a)$	$P_4'=0.3138(2\pi/a)$
$P_5=0.6613$	$P_5'=0.5892$
$P_6=1.4820$	$P_6'=1.14985$
$P_7=0.39511(2\pi/a)$	$P_{11}=0.11561(2\pi/a)$
$P_8=0.6809(2\pi/a)$	$P_{12}=0.4522(2\pi/a)$
$P_9=1.9919$	$P_{13}=1.2466$
$P_{10}=2.9516$	$P_{14}=4.257$

[9] S. H. Chen and B. H. Brockhouse, Solid State Commun. **2**, 73 (1964).

[10] S. H. Chen, Ph.D. thesis, McMaster University, 1964 (unpublished).

The parameters P_4, P_5, and P_6 which determine the departures from a regular octahedron, the rounding off of the corners and the slight dimpling of the planes, were found by fitting to the dHvA periods. The values are listed in Table I.

The electron jack satisfies the condition

$$W_J(\mathbf{k})=0, \tag{4}$$

where

$$W_J(\mathbf{k})=|W_0'(\mathbf{k})+1|^{P_{13}}+\sum_{i,j,k=x,y,z}^{\pm\ 6\text{ balls}}|G_{i,j,k}{}^{\pm}(\mathbf{k})+1|^{P_{14}}-1. \tag{5}$$

$W_0'(\mathbf{k})$ has the same functional form as $W_0(\mathbf{k})$ but with parameters P_4', P_5', and P_6'. The function G which describes the balls is defined as

$$G_{i,j,k}{}^{\pm}(\mathbf{k})=(P_{11})^{P_{10}}\Big/\left[(P_7)^{P_{10}}\left|\frac{k_i\pm P_{12}}{k_i\pm P_{12}\pm P_8}\right|^{P_9}+|k_j|^{P_{10}}+|k_k|^{P_{10}}\right]^{-1}. \tag{6}$$

The values of $P_4'\cdots P_{14}$ determined by Girvan *et al.*[8] are listed in Table I.

A Kohn anomaly will occur at a wave vector $\mathbf{Q}$, when the hole octahedron displaced by $\mathbf{Q}$ and the electron jack have a common point of tangency. If the two surfaces intersect each other just at this point of tangency, then the Kohn anomaly will be of the usual type. On the other hand, if the two surfaces intersect in two curves passing through the point of tangency then a cusp-type Kohn anomaly results.

We can determine the position and nature of the Kohn anomalies by determining the locus of intersection between the two surfaces. This locus is found by solving numerically the simultaneous equations

$$W_0(\mathbf{k}+\tfrac{1}{2}\mathbf{G}_{100}-\mathbf{Q})=W_J(\mathbf{k})=0. \tag{7}$$

We confine our interest to values of $\mathbf{Q}$ of the form $\mathbf{Q}=(2\pi/a)(1-\delta, 0, 0)$. The choice $\delta=0$ corresponds to $\mathbf{Q}$ at the H point of the zone. In plotting the locus of intersection it is convenient to project the curves of intersection onto the (k_y,k_z) plane. At $\delta=0$ or $\mathbf{Q}=\frac{1}{2}\mathbf{G}_{100}$, the body of electron jack lies entirely inside the hole octahedron and the only intersections occur where the balls on the electron jack protrude through the hole octahedron. The projection of the locus of intersection with $k_x<0$ for $\delta=0$ takes the form shown schematically in Fig. 1(a); an approximately circular curve centered at the origin and four half circles centered at points along the k_z and k_y axes. The shaded area denotes the region in which $|k_x{}^a|>|k_x{}^b|$, where $|k_x{}^a|$ and $|k_x{}^b|$ are the perpendicular distances to the jack and the displaced octahedron, respectively. The projections for

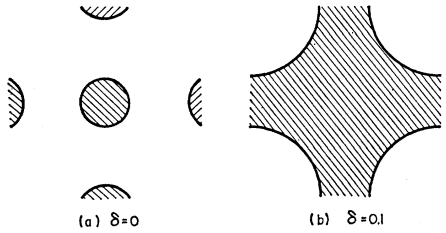

FIG. 1. Schematic projection on the (k_y,k_z) plane of the loci of intersection of the electron jack and the hole octahedron, when the latter is displaced by $(2\pi/a)(1-\delta, 0, 0)$ for (a) $\delta=0.0$; (b) $\delta=0.1$ Shaded areas are those for which k_x is larger for the jack then for the displaced octahedron.

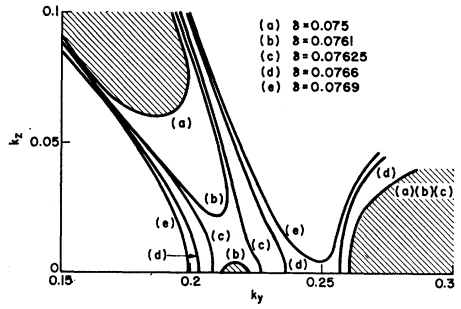

FIG. 3. Close-up showing the connectivity changes in the loci of intersection for values of δ around 0.076.

the final state corresponding to a value of $\delta=0.1$, where the body of the jack has moved through the hole octahedron, is shown in Fig. 1(b). All the curves have fourfold symmetry. Thus in discussing the details of the transition between $\delta=0$ and 0.1 we need only display the positive quadrant in (k_y,k_z) plane.

As we increase δ away from zero the change in the loci of intersection is small at first. At $\delta=0.068$ the first contact between the body of the electron jack and the hole octahedron occurs in the center of the octahedral faces. Thus at $\delta=0.068$ there is a common point of tangency causing a usual Kohn anomaly. In fact, by symmetry, there are four coincident ordinary Kohn anomalies at $\delta=0.068$. The form of the loci of intersection at $\delta=0.07$ is shown in Fig. 2(b). We plot just the loci with negative values of k_x since in the positive direction the hole octahedron and electron-jack surfaces are moving away from each other. At $\delta=0.075$ the shaded region denoting electron protrusion in the center of the face has expanded but there have been no more connectivity changes. However there is a connectivity change between $\delta=0.075$ and $\delta=0.08$ as can be seen from Figs. 2(c) and 2(d). The detailed nature of this change is illustrated in Fig. 3. At $\delta=0.0760$ a small protrusion of the electron jack along the k_y or k_z axis appears, which at $\delta=0.0762$ joins the shaded region in the center of octahedron faces. Then at $\delta=0.07675$ this region joins the shaded region centered at the balls along the $\langle 100\rangle$ directions. When two shaded regions touch there are two curves of intersection passing through a point of tangency causing a Kohn cusp anomaly. Thus there are four coincident ordinary anomalies at $\delta=00761$, eight coincident cusp-type anomalies at $\delta=0.0762$, and four at $\delta=0.0767$.

At $\delta=0.08$ the unshaded region has now shrunk to a roughly circular band around the origin. As δ increases, this band shrinks until contact occurs between the shaded regions along the k_y and k_z axes at $\delta=0.0895$, where there are again four coincident cusp-type Kohn anomalies. Finally, as δ increases further the unshaded region shrinks as shown in Fig. 4 until it disappears althogether at $\delta=0.097$ where there are four coincident ordinary Kohn anomalies. In Table II we list the position and type of the series of Kohn anomalies.

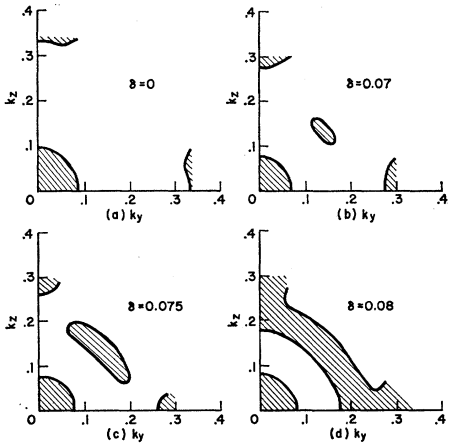

FIG. 2. Projection of the (k_y,k_z) plane of the loci of intersection of the electron jack and the hole octahedron displaced by $(2\pi/a)(1-\delta, 0, 0)$ for various values of δ.

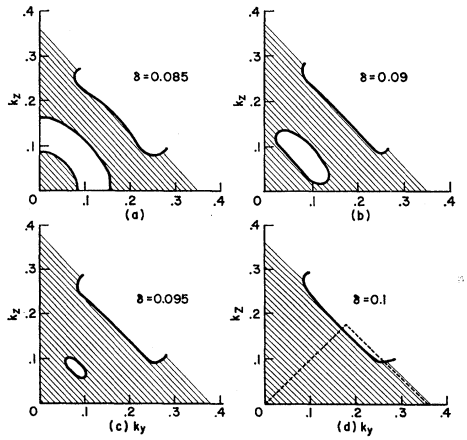

FIG. 4. Projection on the (k_y,k_z) plane of the loci of intersection of the electron jack and the hole octahedron displaced by $(2\pi/a)\times(1-\delta, 0, 0)$ for various values of δ.

TABLE II. Position and nature of the Kohn anomalies in W.

δ	Type	Number of coincident anomalies
0.068	usual	4
0.0760	usual	4
0.0762	cusp	8
0.0768	cusp	4
0.0895	cusp	4
0.097	usual	4

III. ONE-ELECTRON SUSCEPTIBILITY OF W

The one-electron susceptibility $\chi^0(\mathbf{Q})$ is defined, ignoring the matrix elements, as

$$\chi^0(\mathbf{Q})=-\frac{1}{8\pi}\sum_{n,n'}\int d^3k\frac{f(\epsilon_{\mathbf{k}+\mathbf{Q}}{}^n)-f(\epsilon_{\mathbf{k}}{}^{n'})}{\epsilon_{\mathbf{k}+\mathbf{Q}}{}^n-\epsilon_{\mathbf{k}}{}^{n'}}, \quad (8)$$

where $\epsilon_{\mathbf{k}}{}^n$ is the energy of band n and wave vector $\mathbf{k}$ and $f(\epsilon)$ is the Fermi function. In the generalized random phase approximation the static wave-vector-dependent susceptibility is given by $\chi(\mathbf{Q})$, where

$$\chi(\mathbf{Q})=\chi^0(\mathbf{Q})/[1-\bar{V}\chi^0(\mathbf{Q})], \quad (9)$$

and $\bar{V}$ is a constant representing an effective screened Coulomb interaction. The analysis which was carried out in Sec. II gives the position and nature of the nonanalyticities of χ^0 as a function of $\mathbf{Q}$. It is possible in principle to estimate the size of the various nonanalytic contributions using the general formulas derived by Roth *et al.*[4] by calculating the curvatures and velocities. This is not a satisfactory procedure for the case at hand where there is a series of closely spaced anomalies which may interfere and combine with one another. Instead it is preferable to evaluate χ^0 directly by numerical integration. Since we are specifically interested in the fine structure of χ^0 arising because of the "nesting" characteristics of the Fermi surface, a direct numerical attack on Eq. (8) is not advisable. A better procedure is to make use of the fact that the singular contributions come from the region near the Fermi surface and that the integration perpendicular to surface gives only a slowly varying contribution which we can estimate. Thus we perform the perpendicular integration analytically first, and the remaining two-dimensional integration over the nesting portions of the Fermi surface, numerically. This procedure has the two immediate advantages of reducing the dimensionality of the required numerical integration and of changing the singularities in the integration from the x^{-1} type in Eq. (8) to a logarithmic singularity which is much more readily handled numerically.

We evaluate only the contribution from the term in the sum where $n=b$ is the band at the octahedron and $n'=a$ is the band at the jack. We assume that the other bands contribute only a slowly varying background term which we do not attempt to estimate.

We write the equations determining the jack surface as

$$|k_x|=\psi^a(k_y,k_z). \quad (10)$$

Similarily, for the hole octahedron displaced by $\mathbf{Q}$ we can write

$$|k_x|=\psi^b(k_y,k_z)+\delta. \quad (11)$$

Now in the neighborhood of the Fermi surface we can expand the energy spectrum for the electron jack, measured from the Fermi energy

$$\epsilon^a(k_x,k_y,k_z)=v_x{}^a(k_y,k_z)[k_x-\psi^a(k_y,k_z)]+O([k_x-\psi^a(k_y,k_z)]^2). \quad (12)$$

To obtain the correct behavior for the nonanalytic contribution it is sufficient to keep just the first term in this expansion. By the same token, we can cut off the integration over k_x in Eq. (8) at a constant distance from the Fermi surface. Furthermore, the x component of the velocity is approximately constant over the region of interest to us, namely, the body of the electron jack, so we may replace $v_x{}^a(k_y,k_z)$ by a constant value $v_x{}^a$. We may make a similar expansion for the hole octahedron.

The integration over k_x in Eq. (8) may be performed at once and we obtain the result at $T=0°\mathrm{K}$, that

$$\chi^0(\delta)=\frac{1}{4\pi^3|v_x{}^a-v_x{}^b|}\int_A dk_y dk_z \times\{2\ln|b\epsilon_0|-\ln|\delta+\kappa(k_y,k_z)|-\ln|-\delta+\kappa(k_y,k_z)|\}, \quad (13)$$

where $\kappa(k_y,k_z)$ is the distance in the k_x direction between the jack and the octahedron with $\delta=0$:

$$\kappa(k_y,k_z)=\psi^a(k_y,k_z)-\psi^b(k_y,k_z). \quad (14)$$

The energy ϵ_0 in the first term is the lower cutoff energy and $b=(v_x{}^a-v_x{}^b)/v_x{}^a v_x{}^b$. This first term is a constant independent of δ. The second and third terms arise from the front and back surfaces, respectively. The nonanalytic structure in χ^0 arises from the third term.

The region of integration A in (13) must be chosen to include all the Fermi surface contributing to the Kohn anomalies but to exclude any regions where either Eq. (10) or Eq. (11) has no root. A suitable choice for A is a square with diagonals of length $0.68\times(2\pi/a)$, along the k_y and k_x axes. By symmetry it is sufficient to compute the integral over one eighth of the square. The integration was thus performed over the triangle enclosed by the dashed line in Fig. 4(d). We took a mesh of approximately 1200 points in the region A, computed numerically the values of κ at these points, and then evaluated the integral (13). In order to eliminate the region where ψ^b is multivalued we found it convenient to replace the ball along the negative k_x direction by a paraboloid of revolution. Since the important intersections occur on the body of

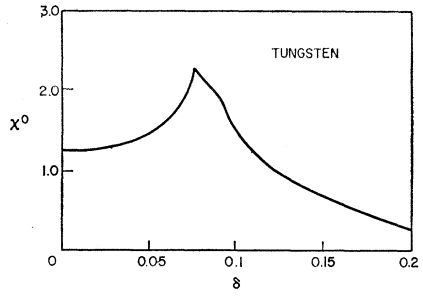

FIG. 5. One-electron susceptibility χ^0, in units of the density of states of the body of jack (=0.028 states of one spin per eV atom), as a function of δ.

the jack, this approximation should not be serious except for values of δ near $\delta=0$.

The results of computations are shown in Fig. 5. We have expressed the results in units of the density of states of the body of the jack. We have estimated the first term using the values $\epsilon_0=1.3$ eV and $v_x{}^a\approx -v_x{}^b \approx (8.2\text{ eV})/(2\pi/a)$. These values we estimated from Mattheiss's band-structure calculations with the W_2 potential.[11] These calculations give a good Fermi surface and excellent agreement with the total band-structure density of states estimated by MacMillan.[12] Thus we feel confident in using it for the individual pockets.

The results show a single maximum in $\chi^0(\delta)$ occurring at a sharply peaked structure near $\delta=0.076$. The computed values give χ^0 a local minimum at $\delta=0$. This may, however, be an artifact of our approximate treatment of the balls, and it is possible that χ^0 has, in fact, a slight maximum at $\delta=0$. In Fig. 6 we plot the detailed structure in χ^0 for $0.06<\delta<0.1$. The arrows indicate the values of δ at which Kohn anomalies were found in Sec. II. The usual type anomalies at $\delta=0.068$ and $\delta=0.097$ show up only weakly. The cusp-type anomalies at $\delta\simeq 0.076$ show up strongly but less so at $\delta\simeq 0.0895$. The calculated values are, of course, too coarse to show the very detailed fine structure we found in Sec. II near $\delta=0.076$. The composite singularity shows up as a sharp cusplike peak in χ^0. The other cusp anomaly at $\delta=0.0895$ shows as a break in the slope of χ^0 but does not correspond to a maximum in χ^0.

It is possible to extend the calculation to finite temperature and observe the smearing of the peak. Since we wish to do one integration analytically it, is convenient to make the "slanting" approximation to the Fermi function

$$\begin{aligned} f(\epsilon)&=1, && \epsilon<-CT \\ &=(CT-\epsilon)/2CT, && -CT<\epsilon<CT \\ &=0, && \epsilon>CT \\ C&=2.6k_B. \end{aligned} \tag{15}$$

[11] L. F. Mattheiss, Phys. Rev. **139**, A1893 (1965).
[12] W. L. McMillan, Phys. Rev. **167**, 331 (1968).
[13] T. M. Rice and B. I. Halperin (unpublished).

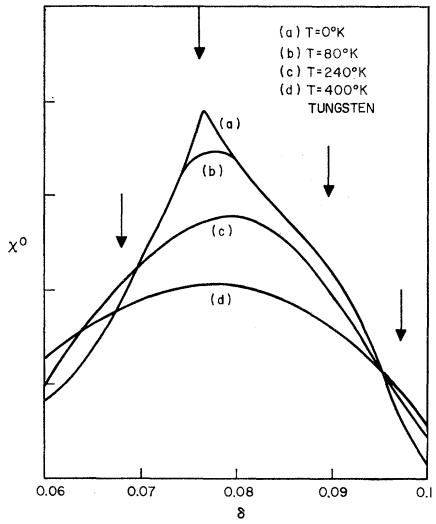

FIG. 6. Temperature dependence of the peak in $\chi^0(\delta)$.

The constant C was chosen to reproduce the correct linear temperature coefficient of a cusp-type Kohn anomaly.[13] Substituting in Eq. (8) we find

$$\chi^0(\delta,T)=\frac{1}{|v^a-v^b|}\cdot\frac{1}{4\pi^3}\Sigma_\pm\int_A dk_y dk_z$$
$$\times\Big(\ln|b\epsilon_0|+1-\ln|bCT+\kappa\pm\delta| + \frac{1}{2bCT}(bCT-\kappa\mp\delta)\ln\left|\frac{bCT+\kappa\pm\delta}{-bCT+\kappa\pm\delta}\right|\Big). \tag{16}$$

The results for values of $T=80$, 240, and 400°K are shown in Fig. 6 for the region $0.06<\delta<0.1$. Outside of the region the temperature dependence is very small. In Fig. 7 the maximum value of χ^0 is plotted versus temperature. The initial temperature dependence is linear for the region $T\lesssim 100$°K and for larger temperatures it falls off more slowly.

It is interesting to compare the properties of W with those we infer from the antiferromagnetism in Cr.

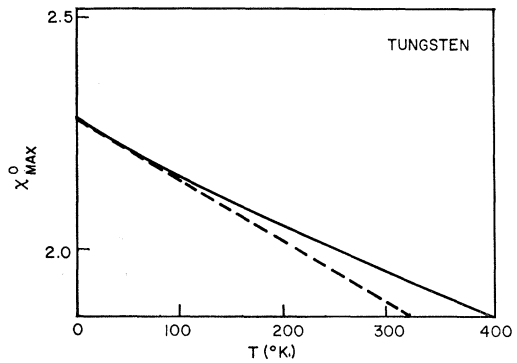

FIG. 7. Maximum value of $\chi^0(\delta)$ as a function of temperature.

First, if W were antiferromagnetic, then T_N would be determined according to the generalized RPA, by the condition

$$1/\bar{V}=\chi_{\max}{}^0(T_N), \tag{17}$$

where $\chi_{\max}{}^0$ is the maximum value of $\chi^0(\delta)$. (We have assumed a second-order transition.) If we assume that the left-hand side varies linearly with external perturbations, such as pressure, and we neglect the explicit dependence of χ^0 on the perturbation, then we see at once from Fig. 7 that the qualitative behavior of $T_N(P)$ would be similar to that observed in Cr and its alloys.[6,7] The Néel temperature would drop more rapidly at higher values of T_N and would go to zero linearily with pressure. We believe that inclusion of the explicit dependence of χ^0 on P would not qualitatively alter this picture.

A second comparison we can make is with the nesting qualities of Cr. In W, knowing the Fermi surfaces and the velocities we can compute the energy gap which would be necessary in W in order to annihilate large portions of the Fermi surface as happens in Cr. In the commensurate phase this energy gap is $2\Delta_W{}^C=2b^{-1}\delta_0 \approx 0.8$ eV, where $\delta_0\approx 0.1$ is the average distance between the surfaces along a line in the (100) direction when $\delta=0$. This value of the gap is roughly twice that found by Barker in commensurate Cr alloys ($2\Delta_{\mathrm{Cr-Mn}}\simeq 0.35$ eV).[7,14] On the other hand, for the incommensurate phase the necessary energy gap is $2\Delta_W{}^I=2b^{-1}\delta_1=0.12$ eV, where $2\delta_1$ is the separation between the first and last ordinary Kohn anomalies. This gap is not significantly different from that observed in Cr by Barker, Halperin, and Rice[15] ($2\Delta_{\mathrm{Cr}}\simeq 0.12$ eV). We conclude therefore that the reason why Cr is antiferromagnetic but W is not antiferromagnetic, is not primarily due to the better matching or nesting in Cr, but is due to the larger interaction strength relative to band width in the $3d$-transition series.

IV. PHONON SPECTRUM OF W

The phonon spectrum of W has been measured using neutron diffraction by Chen and Brockhouse.[9,10] They found an anomalous dip near the H point in the zone such that the phonon spectrum had a local minimum at H rather than a maximum as in other bcc metals, e.g., Nb,[16] Na.[17] Their measurements, however, were taken on a relatively coarse scale in wave-vector space. In the region of interest to us they have points only at $\delta=0.0$, 0.1, and 0.2. Thus, they have not measured them on a sufficiently fine scale to resolve the detailed structure which we are interested in.

It is a difficult task to calculate *ab initio* the phonon spectrum of a transition metal. There will be, however, a term proportional to the electronic polarizability which will involve χ^0. We therefore interpolate between the measured values using a form

$$\omega^2(\delta)=B-A\chi^0(\delta,\omega), \tag{18}$$

where $\omega(\delta)$ is the frequency of the longitudinal mode along ΓH. We confine our attention to the longitudinal phonon spectrum. Similar estimates can be made for the transverse modes but the effect appears to be less dramatic for the transverse modes. Since we fit only over a limited region of $0<\delta<0.2$, we take A and B to be constants independent of δ. Strictly speaking, A should also depend on χ^0 through the enhancement factor. However, the enhancement factor for the polarizability will be less than that for the susceptibility and could even be less than one. This form with two adjustable parameters gives a reasonable fit to the three experimental points. It is usually an excellent approximation for phonon calculations, to replace $\chi^0(\delta,\omega)$ by its static value; however, in the vicinity of the peak there is strong temperature, and therefore energy dependence in χ^0, and we evaluate χ^0 at a frequency $\omega_0/2\pi=5.50\times 10^{12}$ cps, the average phonon frequency near H. The real part of the frequency is given, thus by

$$\mathrm{Re}\omega(\delta)=[B-A\ \mathrm{Re}\chi^0(\delta,\omega_0)]^{1/2}. \tag{19}$$

We may also evaluate the imaginary part $\Gamma(\delta)$ which gives the contribution to the phonon lifetime due to the electronic damping:

$$\Gamma(\delta)=-\mathrm{Im}\omega(\delta)=\tfrac{1}{2}\omega_0 A\ \mathrm{Im}\chi^0(\delta,\omega_0). \tag{20}$$

The finite-frequency susceptibility χ^0 is given by

$$\chi^0(\mathbf{Q},\omega)=\frac{-1}{16\pi^3}\int d^3k(f(\epsilon_{\mathbf{k}+\mathbf{Q}}{}^b)-f(\epsilon_{\mathbf{k}}{}^a)) \times\left(\frac{1}{\omega+\epsilon_{\mathbf{k}+\mathbf{Q}}{}^b-\epsilon_{\mathbf{k}}{}^a-i\epsilon}-\frac{1}{\omega-\epsilon_{\mathbf{k}+\mathbf{Q}}{}^b+\epsilon_{\mathbf{k}}{}^a+i\epsilon}\right). \tag{21}$$

Proceeding as in Sec. III we find at $T=0$°K

$$\mathrm{Re}\chi^0(\delta,\omega_0)=\frac{1}{16\pi^3 v}\sum_{\eta=\pm1;\eta'=\pm1}\int_A dk_y dk_z\{\ln(b\epsilon_0) -\ln|\kappa(k_y,k_z)+\eta\delta+\eta'\omega_0/v|\}, \tag{22}$$

where for simplicity we have written $v_x{}^a\simeq -v_x{}^b=v$. The ratio ω_0/v is quite small, and $\mathrm{Re}\chi^0(\delta,\omega_0)$ calculated from (22) is just the average of the static susceptibilities at $\delta\pm 0.003$. Thus the finite ω corrections are only of consequence very near the peak at $\delta=0.076$ and correspond to rounding it out over a width of 0.006, approximately.

Evaluating Eq. (22) and adjusting the parameters A and B we obtain the phonon spectrum shown in Fig. 8. The form for $\omega(\delta)$ that we have chosen attributes the

[14] A. S. Barker and J. A. Ditzenberger (unpublished).
[15] A. S. Barker, B. I. Halperin, and T. M. Rice, Phys. Rev. Letters **20**, 384 (1968).
[16] Y. Nakagawa and A. D. B. Woods, Phys. Rev. Letters **11**, 271 (1963).
[17] A. D. Woods, B. N. Brockhouse, R. H. March, and A. T. Stewart, Phys. Rev. **128**, 1112 (1962).

whole of the dip in the longitudinal mode near the H point to the rise in χ^0 due to the nesting of the jack and octahedron. The points are taken from the experiments of Chen and Brockhouse.[9,10] The results show a sharp dip in the phonon spectrum centered around $\delta=0.078$. The dip is approximately $0.02(2\pi/a)$ wide and attains a maximum depression of $\approx 0.3\times 10^{12}$ cps. In Fig. 9 we plot in detail the region $0.06<\delta<0.1$ and show also the temperature dependence. This was calculated by methods similar to those employed in Sec. III. This temperature dependence should show up as an anomalous contribution in the vicinity of the dip, in addition to the anharmonic shifts, etc.

Associated with the Kohn anomalies in the real part of the phonon spectrum are anomalous changes in the electronic contribution to the phonon lifetimes. These we have evaluated using Eq. (20). The imaginary part

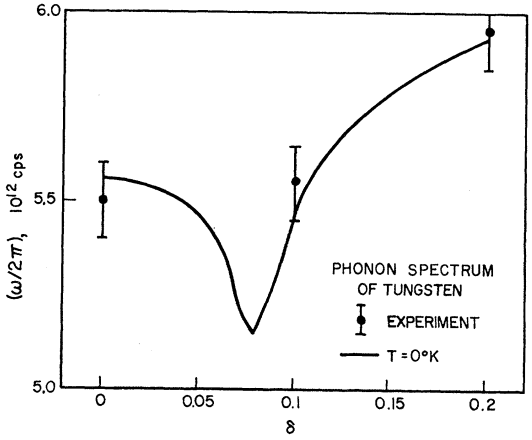

FIG. 8. Longitudinal phonon frequency as a function of δ.

of χ^0 may be written as

$$\mathrm{Im}\chi^0(\delta,\omega_0)=\frac{1}{16\pi^2 v}\sum_{\pm}\int_A dk_y dk_z \times\left[\tfrac{1}{2}(v(\kappa\pm\delta)-\omega_0)-\tfrac{1}{2}(v(\kappa\pm\delta)+\omega_0)\right], \quad (23)$$

where f is the Fermi function. We have evaluated this integral numerically and the corresponding values for $\Gamma(\delta)$ are shown in Fig. 10. These show that at zero temperature there is a very sharp peak in Γ in the region $0.06<\delta<0.1$. For other values of δ, Γ is very small. In the limit $\omega_0\to 0$ one can show that

$$\lim_{\omega_0\to 0}\frac{\mathrm{Im}\chi_0(\mathbf{Q},\omega_0)}{\omega_0}\propto N_{\mathbf{Q}}(\xi=0,\eta=0), \quad (24)$$

where $N_{\mathbf{Q}}$ is the joint density of states

$$N_{\mathbf{Q}}(\xi,\eta)=\sum_{\mathbf{k}}\delta(\xi-\tfrac{1}{2}(\epsilon_{\mathbf{k}+\mathbf{Q}^b}-\epsilon_{\mathbf{k}^a})) \times\delta(\eta-\tfrac{1}{2}(\epsilon_{\mathbf{k}+\mathbf{Q}^b}+\epsilon_{\mathbf{k}^a})) \quad (25)$$

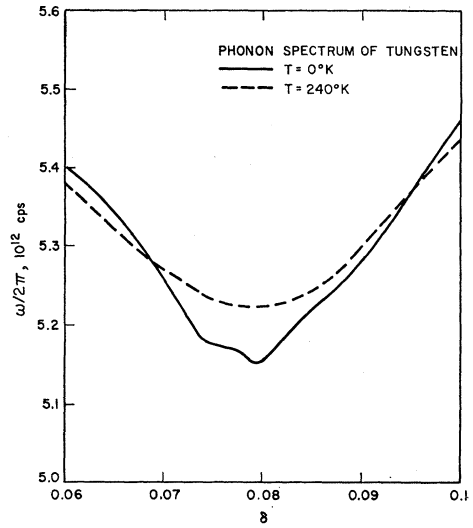

FIG. 9. Predicted temperature dependence of the dip in the phonon frequency.

and at cusp-type Kohn anomaly N has a logarithmic divergence as $\xi, \eta\to 0$.[6,13] This behavior is reflected in the sharp peak in $\Gamma(\delta)$.

As the temperature is raised the peak broadens and reduces in intensity rapidly until at $T=300$°K it takes the form shown in Fig. 10. Note the anomalous behavior in the vicinity of $\delta=0.076$, where the inverse lifetime $\Gamma(T)$ *decreases* as the temperature increases. It may not be possible to observe this experimentally, however, since the contributions to the damping from anharmonic effects or other mechanisms which increase with temperature may be too large. Note also that phonons continue to be well defined. Even at the maximum value of Γ, the ratio Γ/ω_0 only attains a value $\Gamma/\omega_0\approx 0.02$.

It is clear that to resolve this fine structure in the phonon spectrum experimentally a good resolution will be needed simultaneously in both energy and wave vector. From Fig. 8 we see that a resolution of 0.1×10^{12}

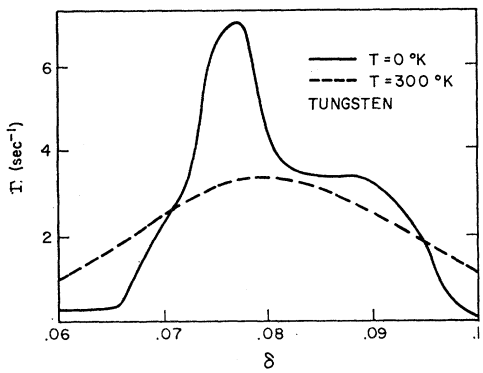

FIG. 10. Predicted inverse lifetime of the longitudinal phonon spectrum due to Landau damping as a function of δ. The imaginary part of the phonon frequency Γ is expressed in units of 10^{11} rad/sec.

cps in energy and $0.01(2\pi/a)$ in wave vector in the ΓH direction are needed. Comparable resolution is needed in the directions perpendicular to ΓH. The conditions for a Kohn anomaly define a surface in $\mathbf{k}$-space, and as the $\mathbf{Q}$ vector moves away from the symmetry direction ΓH, the anomalies which occur in multiples of four by symmetry will split linearly, leading to broadening of the anomalous structure. Thus the resolution needed in the transverse directions is also $\sim 0.01(2\pi/a)$. We should like to point out that calculations reported here for the phonon frequency and damping can be extended to give directly the neutron cross sections for a series of scans through the anomalous region which could then be convoluted with experimental resolution functions and compared directly with experimental counting rates.

V. APPLICATION TO OTHER Cr-GROUP METALS

The detailed structure in χ^0 which we obtained for tungsten depended on the exact nature of the deviations of the hole octahedron and the body of the jack from a perfect octahedron. Although the gross features of the band structure will be similar in Cr and Mo, the nature of these deviations may be quite different. Thus we cannot infer from this work the exact behavior of Cr or Mo. Further, there has been no accurate determination of the Fermi surface of Mo comparable to Girvan, Gold, and Phillips[8] work on W. Thus we cannot make comparison with the recent neutron diffraction studies on Mo of Walker and Egelstaff.[18] The de Haas–van Alphen effect in Cr has been studied extensively by Graebner and Marcus.[19] The antiferromagnetism of Cr greatly complicates the interpretation of the observed periods, however, and the exact shape of the paramagnetic Fermi surface cannot be obtained in this way.

There is, however, one important statement which we can make. We can show that

$$C=U+4, \tag{26}$$

where C and U are the number of Kohn anomalies of the cusp type and of the usual type, respectively, which occur when the body of the electron jack and the hole octahedron pass through one another. This statement implies immediately that $C>0$. Thus there will always occur cusp-type Kohn anomalies, for the Cr-group metals. This conclusion also supports the proposition advanced earlier by the authors,[6,18] that the peak in Cr is occurring at such an anomaly. We can derive Eq. (26) as follows.

Figures 1(a) and 1(b) are schematic views from the [100] direction of the superimposed displaced Fermi surfaces of tungsten at $\delta=0$ and $\delta=0.1$. The shaded area represents the regions where the electron jack protrudes through the hole surface. At $\delta=0$ there are five disconnected shaded areas in the picture, while at $\delta=0.1$ there is a single shaded area, embedded in a white frame. As δ increases from 0 to 0.1, the shaded area grows monotonically while the white area shrinks.

Let $N(\delta)$ be the number of disconnected shaded areas minus the number of white areas at the given value of δ. The number $N(\delta)$ will increase by unity as δ increases, if there is an ordinary Kohn anomaly, i.e., if a shaded area shrinks to zero, or if a white area appears in the center of a shaded area. On the other hand, $N(\delta)$ will decrease by unity if there is a cusp-type Kohn anomaly, i.e., if two shaded areas touch and fuse into one, or if one white area splits into two white areas. Since $N(0)=4$ and $N(0.1)=0$, we have proved Eq. (26).

VI. CONCLUSIONS

In this paper we have carried out an analysis of the peak in $\chi^0(\mathbf{Q})$ arising from the nesting electron and hole surfaces of W. The methods we have used have been tailored to determine the detailed form of the peak. They do not answer the question as to whether this peak is the absolute maximum of χ^0 or just a local maximum. To answer this question a complete evaluation of Eq. (8) is necessary such as that carried out for Cr, Eu, and other rare earth metals by Evenson and Liu.[1] In these latter analyses the right-hand side of Eq. (8) was numerically integrated over the Brillouin zone. Their mesh, however, is too coarse to resolve in detail the sort of fine structure which we have been discussing. The two types of analysis are therefore complementary: one gives the over-all variation of background term in χ^0, while the other gives the detailed shape of the rapid variation occurring near Kohn anomalies.

A knowledge of the detailed behavior of χ^0 is necessary to study band-structure effects on itinerant magnetic transitions. In this connection it would be interesting to study the detailed shape of the Kohn anomalies in the phonon spectrum also in Cr. Of course, in Cr such a study should be done above the Néel temperature of 312°K. It may be possible to get more detail by doping with a small amount of V, which will reduce T_N, although at the cost of some rounding of cusps due to scattering.

[18] C. B. Walker and P. A. Egelstaff, Phys. Rev. **177**, 1111 (1969).
[19] J. A. Graebner and J. Marcus, Phys. Rev. **175**, 659 (1968).